In-situ Cu-doped MnCo-spinel coatings for solid oxide cell interconnects processed by electrophoretic deposition

Elsevier Editorial System(tm) for Ceramics International

Manuscript Draft

Manuscript Number: CERI-D-19-04349R2

Title: In-situ Cu-doped MnCo-spinel coatings for solid oxide cell interconnects processed by electrophoretic deposition

Article Type: Full length article

Keywords: coating; spinel; EPD; solid oxide cell

Corresponding Author: Dr. federico smeacetto, PhD

Corresponding Author's Institution: Politecnico di Torino

First Author: Antonio Sabato

Order of Authors: Antonio Sabato; Sebastian Molin; Hassan Javed; Elisa Zanchi; Aldo R Boccaccini; federico smeacetto, PhD

Abstract: The Cu doping of the Mn-Co spinel is obtained "in-situ" by electrophoretic co-deposition of CuO and $Mn_{1.5}Co_{1.5}O_4$ powders and subsequent two-step reactive sintering. Cu-doped $Mn_{1.5}Co_{1.5}O_4$ coatings on Crofer22APU processed by electrophoretic co-deposition method are tested in terms of long term oxidation resistance and area specific resistance tests up to 3600 hours. The introduction of Cu in the spinel lead to higher level of densification of coatings for all the considered aging periods at 800°C and stabilizes the cubic phase of the $Mn_{1.5}Co_{1.5}O_4$ spinel. Corrosion rate of the Cu-doped $Mn_{1.5}Co_{1.5}O_4$ coated Crofer22APU is ~10x lower than for the uncoated Crofer22APU. The stabilization of the cubic phase due to Cu doping, which reduces the extent of the tetragonal-cubic phase transition and limits possible thermal stresses due to mismatch of coefficients of thermal expansion or volume changes, is reviewed and discussed by means of electrical conductivity measurements together with diffraction patterns and elemental analyses. These novel electrophoretic co-deposited Cu-doped MnCo spinel coatings represent an innovative approach to obtain coatings with higher density and have future applications in the view of reaching lower rates of Cr evaporation form the steel.

Cover Letter

POLITECNICO
DI TORINO
Department of Energy

Associate Professor
Federico Smeacetto, PhD

Torino, June 16th, 2019

To the Editor of ***Ceramics International***

OBJECT: Submission of the revised paper "In-situ Cu-doped MnCo-spinel coatings for solid oxide cell interconnects processed by electrophoretic deposition"

Dear Editor,

We have considered the Reviewers' comments to our paper, enclosed in your e-mail message of June 15th, 2019.

First of all, we wish to thank you and the reviewer for the attention dedicated to the revision of the paper. We have reviewed the paper taking into account the Reviewer's comments; reviewed parts are highlighted in red in the revised manuscript.

We sincerely hope that this work can be published on your Journal to have a wide diffusion through the Scientific Community.

Best Regards,

Prof. Federico Smeacetto,

on behalf of all Authors

Department of Energy
Politecnico di Torino Corso Duca degli Abruzzi, 24 – 10129 Torino – Italia
tel: +39 011.090.4756
federico.smeacetto@polito.it

response to reviewers

Reviewer #1: All the comments and suggestions from the review have been properly addressed by the authors in the revised version of the manuscript. However, one minor correction is still needed. Although the authors have added the journal titles to references [21] and [22] in their response to the review, it appears that the revised version of the manuscript itself is still missing this information.
In conclusion, I recommend this paper for publication in Ceramics International.

R: Journal names have been provided also in the manuscript

[21] S. Molin, Evaluation of electrodeposited Mn-Co protective coatings on Crofer 22 APU steel, Int Journal of Applied Ceramic Technology (2017) 349–360. doi:10.1111/ijac.12816.

[22] S. Molin, A.G. Sabato, H. Javed, G. Cempura, A.R. Boccaccini, F. Smeacetto, Co-deposition of CuO and Mn1.5Co1.5O4 powders on Crofer22APU by electrophoretic method: Structural, compositional modifications and corrosion properties, Materials Letters 218 (2018) 329–333.

In-situ Cu-doped MnCo-spinel coatings for solid oxide cell interconnects processed by electrophoretic deposition

A. G. Sabato[1], S. Molin[2], H. Javed[1], E. Zanchi[1], A.R. Boccaccini[3], F. Smeacetto[4]*

1. Department of Applied Science and Technology, Politecnico di Torino, Corso Duca degli Abruzzi 24, 10129 Torino, Italy

2. Faculty of Electronics, Telecommunications and Informatics, Gdańsk University of Technology, ul. G. Narutowicza 11/12, 80-233 Gdańsk, Poland

3. Department of Materials Science and Engineering, University of Erlangen-Nuremberg, Cauerstr. 6, 91058 Erlangen, Germany

4. Department of Energy, Politecnico di Torino, Corso Duca degli Abruzzi 24, 10129 Torino, Italy

Abstract

The Cu doping of the Mn-Co spinel is obtained “in-situ” by electrophoretic co-deposition of CuO and $Mn_{1.5}Co_{1.5}O_4$ powders and subsequent two-step reactive sintering. Cu-doped $Mn_{1.5}Co_{1.5}O_4$ coatings on Crofer22APU processed by electrophoretic co-deposition method are tested in terms of long term oxidation resistance and area specific resistance tests up to 3600 hours. The introduction of Cu in the spinel lead to higher level of densification of coatings for all the considered aging periods at 800°C and stabilizes the cubic phase of the $Mn_{1.5}Co_{1.5}O_4$ spinel. Corrosion rate of the Cu-doped $Mn_{1.5}Co_{1.5}O_4$ coated Crofer22APU is ~10x lower than for the uncoated Crofer22APU. The stabilization of the cubic phase due to Cu doping, which reduces the extent of the tetragonal-cubic phase transition and limits possible thermal stresses due to mismatch of coefficients of thermal expansion or volume changes, is reviewed and discussed by means of electrical conductivity measurements together with diffraction patterns and elemental analyses. These novel electrophoretic co-deposited Cu-doped MnCo spinel coatings represent an innovative approach to obtain coatings with higher density and have future applications in the view of reaching lower rates of Cr evaporation form the steel.

Keywords: coating; spinel; EPD; solid oxide cell

* Corresponding Author: federico.smeacetto@polito.it; Tel 0039 011 0904756

1. Introduction

Solid oxide cells (SOC) technology represents a promising and efficient approach for energy and/or hydrogen production. The working principle of these devices is based on electrochemical reactions between a fuel and an oxidant in a cell, composed of two porous electrodes (anode and cathode) separated by a solid electrolyte. The interconnects are used for separation of gas compartments of the neighbouring cells and electrically connect cells in the stack [1,2]. In planar stack designs, Cr-containing alloys are used as interconnect materials [3]. Ferritic stainless steels such as Crofer22APU, Crofer22H or AISI441 are the most commonly used to date, with a Cr content between 17 wt.% and 23 wt.%. These materials are exposed to the typical severe SOC operating conditions (i.e. 700-900 °C, oxidising and reducing atmospheres for at least 40,000 h with possible intentional and unintentional thermal cycles) [1,2,4–6]. These challenging operating conditions lead to the necessity to protect the interconnect with coatings that should act as physical barriers between the metal and the oxidising atmosphere at high temperatures, limiting the oxygen diffusion towards the interconnect and the Cr evaporation from it [7–9]. In the first case an excessive oxidation could lead to a surface oxide scale which is too thick (in the case of Cr-containing steels, mainly made of Cr_2O_3 and $(Mn,Cr)_3O_4$). High scale thickness may produce spallation effects (with consequent corrosion phenomena of the steel) [6,10,11] and excessively increase the area specific resistance (ASR) of the interconnect, lowering the stack efficiency [6,12,13]. On the other hand, the evaporation of Cr from metallic interconnects is well known to be detrimental for the cathode (cathode poisoning) [14–16]. Both these effects can compromise the durability and the efficiency of cells in the stack. Therefore, an effective protective coating should limit these phenomena (thanks to an appropriate thickness and densification). Moreover, a good coating should also be electrically conductive as well as thermochemical and thermomechanical compatible with the substrate. The latter is particularly important when we consider the typical operating conditions and possible thermal cycling to which these devices are subjected [7,8].

Among the most promising materials for the oxygen side, MnCo-spinel based coatings represent an effective protective solution, thanks to their high electrical conductivity and suitable coefficient of thermal expansion (CTE) [17,18]. In the last decade, few studies have focused on the deposition of these spinels by electrophoretic deposition (EPD) [12,18–26].

EPD has recently gained a strong interest in the fields of advanced ceramics processing and coatings deposition [27–29]. Its popularity is due to its cost effectiveness and simple set-up as well as to the possibility to deposit several materials even on complex shaped substrates and to produce graded or multi-layered coatings [27–29]. Through the use of this technique, in SOC protective coatings technology, it has been possible to obtain coatings with suitable thickness and high densification (necessary to limit the O and Cr diffusion) after post-deposition sintering treatments [26,30].

Several efforts have further been made to improve the properties (i.e. densification or electrical conductivity) of MnCo-spinel based coatings by doping with transition metals such as Fe, Cu or Ni [15,19,20,31–40]. The doped spinels are often produced by “ex-situ” processes, in which doped powders are first produced and then deposited. For powder synthesis methods such as sol-gel, precipitation or mechano-chemical syntheses are used [32,34–38,41]. These methods are energy intensive and time consuming. The approach presented in this work evaluates the possibility to form Cu-doped spinels in-situ, by a single co-deposition process. The idea behind proposing this solution is that commercially manufactured powders, which are produced in large quantities can be used and tailored specifically for applications at the point-of-fabrication by appropriate co-doping with secondary phases. Thus, there is no need to produce new powders in large quantities. This approach might be beneficial in several aspects and is interesting to evaluate scientifically.

Addition of Cu is reported to enhance the densification and the electrical conductivity of undoped MnCo-spinel based coatings [35,37,39,42]. For example, Brylewski et al. [39] studied the effect of different amounts of Cu as dopant in $Mn_{1.25}Co_{1.75}O_4$ and found that the doping enhanced the electrical conductivity, increased the CTE of the spinel from 13.8 $x10^{-6}$ K^{-1} ($Mn_{1.25}Co_{1.75}O_4$) to 14.8 $x10^{-6}$ K^{-1} ($Cu_{0.5}MnCo_{1.5}O_4$) and increased the relative density from ~88% ($Mn_{1.25}Co_{1.75}O_4$) to ~97% ($Cu_{0.5}MnCo_{1.5}O_4$). Szymczewska et al. have shown, using model thin films, that partial substitution of Co by Cu in MnCo2O4 spinel results in increased grain growth/densification of the spinel [33]. Other materials focused studies including the evaluation of Fe,Cu doping of the spinel were performed by Masi et al [37,43]. Authors also pointed towards the possibility of tailoring the chemical composition of the spinels for designing materials for specific purposes/interconnect steels.

However, to the authors best knowledge, there is a lack of studies of protective coatings based on these modified materials, on the performances and possible interactions with the substrates of doped coatings for long periods (more than 1000h) and the effect of doping on long term performances. For example, Talic et al. [19] found that there are no appreciable beneficial effects of Cu and Fe doping of $MnCo_2O_4$ on ASR and oxidation resistance in long term test (more than 4000h). However, they also found that the reaction layer between the steel and the coatings is limited in presence of doping for long term oxidation at 900°C.

The present study extends our previous investigation on Cu-doped MnCo spinel based coatings [22]. It is focused on the evaluation of performances of Cu doped $Mn_{1.5}Co_{1.5}O_4$ coatings in long term oxidation resistance (up to 3000h) and ASR tests (up to 3600h). As described in [22] the studied coatings were produced by an electrophoretic co-deposition of CuO (in different amounts: 5 wt.% and 10 wt.%) and $Mn_{1.5}Co_{1.5}O_4$; the doping of the spinel was then obtained “in-situ” by reactive sintering. The compatibility between these coatings and the substrates after the tests is assessed and discussed together with the oxide scale growth and the Cr-diffusion. The co-

deposition and in-situ doping of MnCo-spinel approaches offer a flexible and versatile method, allowing to save time and lowering the costs of this process compared to the “ex-situ” methods mentioned above. The aim of this paper is to investigate the effect of the Cu-doping on the long term stability of the Mn-Co based coatings, obtained with EPD co-deposition and in situ doping, with respect to their effectiveness in providing corrosion protection and Cr diffusion limitation.

2. Experimental

Undoped and Cu-doped $Mn_{1.5}Co_{1.5}O_4$ coatings were deposited on Crofer22APU substrates by using EPD. $Mn_{1.5}Co_{1.5}O_4$ powders from American Elements (USA) were used to produce the spinel coatings, while CuO powders from Alfa Aesar were used as dopant precursor during the co-deposition. The suspension was composed of a solution of deionized water and ethanol (EtOH/H_2O 60/40 vol.%) as dispersant medium; the overall solid content was 37.5 gr L^{-1}. This parameter was maintained constant for all the depositions, varying the relative wt% of $Mn_{1.5}Co_{1.5}O_4$ and CuO in order to obtain different doping levels. Three different amounts of CuO were considered: pure spinel (0 wt% CuO) as a benchmark, 5 wt% CuO and 10wt % CuO. The obtained coatings were labelled respectively MCO, 5CuMCO and 10CuMCO. The deposition was carried out for 20 seconds with a constant applied DC voltage of 50 V. The different suspensions were maintained under magnetic stirring and subjected to sonication before each deposition in order to ensure high homogeneity and avoid possible sedimentation phenomena. Dynamic light scattering (DLS) was used to determine the size distributions and Z potential of MCO and CuO powders in a 60%Ethanol-40%H_2O solution by a Malvern Zetasizer Nano Series instrument.

The theoretical compositions of the Cu-modified spinel coatings can be calculated balancing the cations fractions in the EPD suspensions and assuming that MCO and CuO powders deposit homogeneously and completely react during sintering. In this regard, 5CuMCO suspension corresponds to $Mn_{1,43}Co_{1,43}Cu_{0,14}O_4$ (Cu/(Mn+Co+Cu) = 0,047), whereas 10CuMCO to $Mn_{1,35}Co_{1,35}Cu_{0,30}O_4$ spinel (Cu/(Mn+Co+Cu) = 0,1).

The Crofer22APU substrates were used as counter electrodes during EPD and the distance between the electrodes was fixed at 1 cm. Crofer22APU substrates were cleaned in an ultrasonic bath with acetone before the deposition. Two different coupon shapes were considered as substrates, respectively for the oxidation resistance (OR) and area specific resistance (ASR) tests. In the first case 2 x 2 cm^2 Crofer22APU coupons were coated on both sides (the deposition was carried out on one side and later on the other side rotating the sample of 180°). 5 samples for each variant (MCO, 5CuMCO and 10CuMCO) were produced in this case, to include multiple samples for reproducibility, in addition 5 bare Corfer22APU coupons were included as reference. For the ASR measurements, rectangular samples were considered (4 x 2 cm^2 with active area 2 x 2 cm^2),

and the deposition was carried out only on one side. The deposition proved to be cathodic for all the three studied suspensions (powders depositing on the negative electrode), thus demonstrating that both the MCO and CuO powders develop a positive surface charge when dispersed in the EtOH/H_2O suspension (pH=7.5).

As deposited coatings were sintered following a two step-sintering procedure: 900 °C for 2 h in Ar/H_2 (5 vol% of H_2) followed by a second step at 900 °C for 2 h in static air. The first treatment (in reducing atmosphere) aimed at the formation of metallic Co and Cu; the formation of metallic species had the purpose to promote higher coatings densification and facilitate the doping of $Mn_{1.5}Co_{1.5}O_4$ spinel with Cu during the following re-oxidation step in air [23]. The oxidation resistance test was carried out exposing the samples at 800 °C in air in a chamber furnace for 3000 hrs. Each sample was cyclically weighed (0.1 mg accuracy, Mettler Toledo XP204 balance) every 250 hours and selected samples were removed from the furnace after different aging periods (e.g. 1000 and 3000h) for subsequent analyses. Cross-scale electrical resistivity measurements (represented by Area Specific Resistance - ASR) were carried out for ~3600 hours at 800 °C. Coated and uncoated steel coupons were sandwiched with (La,Sr)MnO_3 contacting elements and were measured under constant current load of 500 mA cm^{-2} [19,34].

Morphological and chemical analyses were carried out for the as-prepared sample and samples after aging for 1000 h and 3000 h respectively. These investigations were performed using Hitachi TM3000 Scanning Electron Microscope with a backscatter electron detector (BSD). The SEM/EDS analyses were performed on both surfaces (top-views) and polished cross sections of the samples. In latter case the samples were embedded in epoxy resin and polished (using Struers EpoFix epoxy and polishing consumables with final polishing step of 1 µm). The same samples were studied by X-ray diffractometry (Bruker D8 Advance system with CuK_α radiation) in 2θ configuration (20-70°, with a step size of 0.01° and a collection time per step of 2 sec).

In order to study the effects of Cu content on the sintering and electrical conductivity of the spinel, pellets were prepared by mixing $Mn_{1.5}Co_{1.5}O_4$ and CuO in different amounts (0 wt%, 5 wt% and 10 wt% of CuO) reproducing the composition of the used EPD suspensions. Weighed powders were ball milled overnight with 3 mm zirconia balls to ensure good mixing/dispersion. The powders were then pressed under 50 MPa in a steel die. The pellets were sintered either in air at 900 °C or with the same procedure used for the EPD coated Crofer22APU coupons (as described above). The electrical conductivity was evaluated by the van der Pauw method in air. Platinum contacts were painted on sample periphery and were connected to platinum wires. Measurements were performed under voltage control working mode under a 50 mV voltage excitation using Keithley 2400 using an automated laboratory-made switching setup. Shrinkage of the samples was measured by analysis of samples diameters before and after sintering using an electronic micro-caliper (Mitutoyo).

3. Results and Discussion

Fig. 1 provides Scanning Electron Microscope (SEM) images of MCO (a) and CuO (b) powders used for the preparation of the EPD suspensions and ceramic pellets. The morphology of the two powders differs considerably. MCO is composed of irregular fragments (150-750 nm, d_{50}=634 nm), whereas CuO particles present a more distinct spheroidal shape (450-700 nm, d_{50}=526 nm).

Figure 1 HERE

Fig. 1. *SEM images of a) MCO and b) CuO powders used for the co-deposition.*

Zeta potential results obtained by DLS analysis of the two studied suspensions (37.5 10^{-3} gL^{-1} at pH=7.5) were found to be +13 mV for MCO and around +6 mV for the CuO powders, thus determining a cathodic EPD co-deposition mechanism.

Based on the mixed powders, properties of the sintered pellets and protective coatings were evaluated. Producing doped spinels “in-situ” after the co-deposition gives a broad doping range possibility and as an important merit, the doping phase can be selected among other materials, which will be evaluated in future works (e.g. Fe_2O_3).

3.1. Densification and electrical conductivity of Cu doped $Mn_{1.5}Co_{1.5}O_4$ pellets

Based on the results obtained after sintering of the MCO, 5CuMCO and 10CuMCO pellets in air, the addition of copper clearly improved the sinterability of the spinels. MCO pellet shrank (linear shrinkage values are given) ~5.8%, 5CuMCO shrank by 6.6% and 10CuMCO shrank by 10.6% after sintering at 900 °C for 2h. The addition of copper is thus beneficial for obtaining denser microstructures of spinels. In general, it was hard to prepare high quality pellets sintered in a reducing-oxidizing procedure. Large volume changes caused by sequential reduction and oxidation caused severe cracking of the pellets. Only pure MCO and 10CuMCO pellets were obtained with high quality (with no visible cracks) and measured electrically.

Fig. 2 summarizes the results of the electrical conductivity (σ) measurements on the obtained pellets. The collected conductivity values together with the temperature profile as a function of time are reported in **Fig. 2a** and **Fig. 2b**, respectively, for MCO and 10CuMCO. The values of σ vs. T

are shown in **Fig. 2c**. Following the conductivity data of MCO upon cooling, a clear change in the slope is visible around 550-600°C. It corresponds to the phase transition of the spinel, changing from cubic at high temperatures to a mixture of tetragonal and cubic at lower temperatures. This transition seems to be suppressed in the case of Cu-doped spinel, which should be treated as a beneficial effect; though the overall conductivity of the Cu doped sample is lower than conductivity of the undoped spinel, it must be noted that the level of conductivity is still much higher than the required one [44]. The same behaviour is evident observing **Fig. 2a** and **Fig. 2b**: in the case of MCO σ decreases faster with the decreasing of T at T<600°C, the same cannot be said for 10CuMCO. Considering a polaron hopping conduction mechanism, Arrhenius plots can be constructed in accordance with the following equation:

$$\sigma = \frac{A}{T}\exp\left(\frac{-E_a}{kT}\right) \quad (1)$$

where A is a pre-exponential factor [S cm^{-1} K], T is the absolute temperature [K], k is the Boltzmann constant [eV K^{-1}], E_a is the activation energy for the polaron hopping [eV] and σ is the electrical conductivity (S cm^{-1}). The Arrhenius plots (Ln (σT) vs. 1000/T) are reported in **Fig. 2d** for both MCO and 10CuMCO. From the slope of the linear interpolation E_a can be calculated.

Sample 10CuMCO follows a single straight line in the Arrhenius plot suggesting one conduction mechanism, whereas for pure MCO two temperature regimes can be differentiated. At lower temperatures (<450 °C) MCO has higher activation energy (~ 0.50 eV), whereas for higher temperatures it is characterized by lower activation energy (~ 0.45 eV). Similar results for pure spinel have been reported also by other authors [45,46]. The change in activation energy and its mechanism is most probably connected to the change of the crystallographic structure. More hopping centres (e.g. Mn^{3+}/Mn^{4+} pairs in the centres of edge-connected octahedra) are available in the cubic structure, as it has been determined previously for the spinels [46,47]. The change in activation mechanism might be also due to change in grain / grain-boundary contributions of the respective phases.

Figure 2 HERE

Fig. 2. *Results of electrical conductivity (σ) collected on the pellets of MCO and 10CuMCO: σ and T vs. time (a and b), σ vs. T (c) and Arrhenius plots (d).*

3.2. Corrosion properties evaluation

In addition to basic studies performed on pellets, Crofer22APU steel interconnect samples coated with the ceramic protective coatings based on spinel by means of EPD were tested more extensively to evaluate their potential to be used practically. In order to determine corrosion

kinetics, i.e. the oxide growth rate, the weight gain of the samples was measured cyclically. In general, the higher the weight gain, the higher the oxidation extent.

Fig. 3 reports the results of the oxidation resistance test. In **Fig. 3A** the average mass gain per unit of area (in mg cm^{-2}) of each type of coating is plotted as function of time, together with the values of bare Crofer22APU. Based on the individual samples measurements, the relative error (based on standard deviation) for the average weight gain was ~10%. Samples showed good reproducibility and small differences might be due to different surface finish, small area differences etc. The mass gain after 3000h results shows a reduction of the weight gain due to the coatings of approximately 3.5 times (from ~0.77 mg cm^{-2} to ~0.22 mg cm^{-2}), thus confirming the effectiveness of these coatings in reducing the oxidation extent of the underlying steel. However, the doping of MCO does not appear to substantially affect the oxidation resistance: no significant differences in the mass gains between the undoped and Cu doped coated samples were observed. All the samples show a parabolic oxidation behaviour as it is in case of diffusion controlled processes. The oxidation rate in this case can be described by the following equation:

$$(\frac{\Delta m}{A})^2 = k_p t + C \qquad (2)$$

where Δm is the mass gain [g], A is the area of the sample [cm^2], k_p is the oxidation rate [$g^2\ cm^{-4}\ s^{-1}$], t is the time [s] and C is an integration constant. It is possible to calculate k_p plotting $(\Delta m/A)^2$ vs. t (**Fig. 3B**), from equation (2). k_p is represented from the slope of the linear interpolation of the points. The k_p values obtained in this way are reported in **Table 1**. In case of coated samples, k_p resulted to be approximately 10 times lower than in case of bare Crofer22APU. The oxidation rates of the Cu-doped coated samples do not significantly differ from the one of pure MCO, in accordance with what was discussed above. In **Fig. 3c** different values of k_p calculated for each oxidation time separately are reported. The instantaneous corrosion rate $k_p(t)$ was calculated by using the following equation:

$$k_p(t) = \frac{1}{t}\left(\frac{\Delta m(t)}{A}\right)^2 \qquad (3)$$

where Δm(t) is the mass gain [g] after time t [s], A is the area of the sample [cm^2].

The graph reveals that no significant changes occurred in the oxidation kinetics over the time. The values of k_p remain almost constant (or even slightly reduce) after the first 500h of aging, suggesting that all the samples reached a steady state during their oxidation process

Figure 3 REVISED HERE

Fig. 3. *Results of oxidation resistance test at 800°C in air: weight gain vs. time (a), weight gain squared vs. time (b) and instantaneous corrosion rate vs. time (c) for bare Crofer22APU (reference) and MCO, 5CuMCO, 10CuMCO coated samples.*

Table 1 HERE

Table 1 *Corrosion rates (k_p) calculated from the slope of the weight gain curves shown in* ***Fig. 3B****.*

3.3. Post-mortem microstructural evaluation

XRD analyses of samples surfaces were performed after different aging periods of the oxidation resistance test: 0h, 1000h and 3000h. The indexed patterns are reported in **Fig. 4**. The presence of both cubic ($MnCo_2O_4$, PDF #023-1237) and tetragonal (Mn_2CoO_4, PDF #077-0471 and #018-0408) phases of the spinel were detected in each diffraction pattern. It is well known that $Mn_{1.5}Co_{1.5}O_4$ is a dual spinel composed by both phases [24]. Furthermore, in none of the collected patterns peaks of the unreacted CuO are present. This suggests the effective doping of the MCO spinel with Cu thanks to the two-steps reactive sintering process. The aging seems to increase the relative amount of the tetragonal phase in all the investigated coatings. The relative intensity of all the peaks related to this phase (marked as T in the figure) progressively increased after aging for 1000h and 3000h. This might be due to diffusion of elements (i.e. Mn) from the steel that stabilize the tetragonal spinel. On the contrary, doping with Cu seems to stabilize the cubic phase. Comparing the patterns of MCO (**Fig. 4a**), 5CuMCO (**Fig. 4b**) and 10CuMCO (**Fig. 4c**) after the same aging periods the intensity of the tetragonal peaks gradually decreases, increasing the amount of Cu. These effects are especially evident observing **Fig. 4d**, which reports a portion (2θ between 28° and 40°) of the patterns related to MCO and 10CuMCO.

The stabilization of the cubic phase due to Cu has been already reported in other studies [22,31,40]. For example, Xu [31] et al. studied $Mn_{1.5}Co_{1.5}O_4$ doped with different amounts of Cu, a similar trend has been found in the XRD pattern of these spinels. This effect may reduce the extent of the tetragonal-cubic phase transition, to which $Mn_{1.5}Co_{1.5}O_4$ undergoes, during heating-cooling around 400°C [18], thus limiting possible excessive thermal stresses due to CTE or volume changes [31]. Furthermore, these findings are coherent with the results discussed in section 3.1 concerning the electrical conductivity. The difference between MCO and 10CuMCO in Fig.2c are related to the limited tetragonal-cubic phase transition in the doped spinel.

Figure 4 HERE

Fig. 4. *XRD indexed patterns for MCO (a), 5CuMCO (b) and 10CuMCO (c) collected after aging for 0h, 1000h, 3000h together with a magnification (2θ 28°-40°) of the spectra of MCO and 10CuMCO (d).*

Fig. 5 compares the SEM (backscattered) micrographs collected after 0h (as-prepared), 1000h and 3000h of aging on the surface of the samples coated with MCO (**Fig. 5 A, B, C**), 5CuMCO (**Fig. 5 D, E, F**) and 10CuMCO (**Fig. 5 G, H, I**). In **Fig. 5 A, D, G** no metallic particles are visible, thus suggesting the effective re-oxidation during the second step of the sintering treatment (900 °C 2h in air). Moreover, all micrographs indicate homogeneity in the composition and morphology of all the investigated surfaces. The surfaces of the coatings seem quite porous. This is however caused by the constrained sintering process, where the ceramics cannot densify fully in all directions due to the non-shrinking substrate restriction, and the outer layer thus seems porous. As will be shown later, the cross-sections show good densification of the coatings. The surface observation confirms the XRD results discussed above, since no residual CuO was present after the sintering treatment as well as after 1000h and 3000h of aging. The introduction of Cu in the spinel phase seems to lead to higher level of surface densification for all the considered aging periods. Addition of Cu leads to formation of denser islands regions in comparison to the non-modified spinels.

Figure 5 HERE

Fig. 5. *SEM images (top-view) of coated samples after different aging periods (0h, 1000h, 3000h): MCO (A, B, C), 5CuMCO (D, E, F) and 10CuMCO (G, H, I).*

One of the main tasks of the applied ceramic coatings is protection against chromium diffusion which can poison the oxygen electrodes. In order to quantify the extent of Cr diffusion, chemical analyses of the surfaces were performed to check how much chromium diffused from the alloy/chromia scale to the surface and how much Cr can be found inside the coatings in the cross-sectional analyses.

Chemical EDS analyses were performed on the areas shown in **Fig. 5**. The results (at. %) are summarized in Table 2. The relative amount of Mn on the surface of the coatings increased after the aging for all the selected samples, suggesting a possible diffusion of this element from the steel towards the surface. All samples contained ~20-21 at. % Mn in the beginning, which has increased

to ~23 at. %, similarly for all samples. This results may explain the increased intensity of the tetragonal peaks in the XRD patterns (**Fig. 4**). Mn-rich spinel phase, e.g. Mn_2CoO_4 is characterized by tetragonal structure, whereas cobalt rich spinels, e.g. $MnCo_2O_4$ have a pure cubic structure, with the intermediate compounds showing mixed phases. Typically, for the uncoated Crofer22APU steels, a mixed Mn-Cr spinel forms on top of chromia due to Mn diffusion, and here, in the case of coated samples, the outwardly diffusing Mn seems to enrich the deposited MnCoCu spinel phase.

The amount of Cr and Fe on the surface of the coatings is negligible (< 0.5 at. %), even after aging for 1000h and 3000h, thus confirming the very good performance of all the deposited coatings as barrier layers against diffusion at operating temperature of 800°C. No considerable differences between Cu-doped and undoped coatings are evident: the addition of Cu did not negatively affect the diffusion-blocking effect of MCO-based spinel coatings produced here.

The presence of Cu in all the doped samples confirms the effectiveness of the EPD co-deposition process. In addition, the increase of the CuO amount in the EPD suspensions leads to a higher level of Cu in the coatings (detected by EDS). The mean Cu content in the 10CuMCO coatings is approximately 1.7 times higher than in 5CuMCO ones. The content of Cu in the coating seems to scale linearly with the content of Cu-phase in the slurry used for the EPD co-deposition. This has been also observed for other contents, showing usefulness of the EPD co-deposition method to produce composite structures.

Furthermore, the content of Cu in the coatings did not show significant changes in terms of at% during the aging (especially in case of 10CuMCO), thus suggesting a high stability of the Cu-doping over the time, despite the long term aging in relevant conditions.

The absence of peaks beholding to CuO in the XRD patterns, together with the homogeneity shown in the SEM pictures (**Fig. 5**) and the corresponding EDS results just discussed, confirm that the Cu entered the spinel structure after the reactive sintering process. This finding is in accordance with our previous study [22]. This behaviour does not seem to change with the aging at 800°C in air.

Table 2 HERE

Table 2 *Results of EDS semi-quantitative analyses collected on the surfaces of the coated samples reported in* ***Fig. 5****.*

The SEM pictures collected on the cross-sections of the samples after different aging periods are reported in **Fig. 6**. The effects of both the aging and doping on the morphology of the coatings can be seen. These results confirm the trend found in **Fig. 5**. As shown in the Fig. 6 a-c, the

introduction of Cu considerably improves the densification already in the as-sintered state. For the non-doped and the 5CuMCO samples some remaining open porosity can be observed. The 10CuMCO sample shows mostly closed porosity, which should be beneficial for protecting against gaseous chromium transport. Microstructure of the 10CuMCO coating, obtained after reduction-re oxidation sintering procedure with the reduction step carried out at 900 °C is similar to the microstructure obtained for pure spinel after sintering at 1000 °C [23]. Thus the addition of Cu leads to lowering of the sintering temperature, which is a beneficial effect as the steel interconnect will oxidize much less at 900 °C than at 1000 °C. As shown by Bobruk et al. [23], oxide scale formed after reactive sintering of $MnCo_2O_4$ at 900 °C was ~0.25 µm thick, whereas for coatings sintered at 1000 °C, the oxide scale thickness almost doubled (~0.45 µm).

Together with an increase in the densification, a decrease of the thickness of the coatings was found: from ~20 µm in the case of as-sintered MCO to ~12 µm in the case of as-sintered 10CuMCO. Decrease of the thickness is connected to materials sintering and decreasing porosity. Furthermore, all the coatings appear to have a homogenous microstructure and chemical composition without presence of any remaining CuO particles, thus confirming the previous discussion on XRD (absence of peaks of CuO) and our previous findings [22]. The two-steps reactive sintering procedure allowed the introduction of the Cu in the spinel structure, thanks to the formation of Co and Cu as metallic species and MnO. The reactive sintering treatment led also to a high degree of densification, likely thanks to the presence of the metallic species. The aging improved the densification of the coatings as well; this is particularly visible in the doped coatings in comparison with the undoped one. Especially after reaching 3000 hours, both the Cu-doped coatings seem dense. The Cr-containing oxide scale is slightly visible as a darker layer at the interface between the steel and the coatings. The reduced thickness of this layer, even after aging for 3000h at 800°C in air, confirms the effectiveness of the produced coatings against the oxidation of the coated Crofer22APU. In **Fig. 6i** (10CuMCO aged 3000h) a crack is visible in the middle of the coating. It seems to form in the porous region, that formed due to pore coalescence. This may be dangerous in real operating conditions: a sudden failure of the coating would expose the underlying steel at the severe operating conditions of a SOC stack. However, the lower part of the coating is still well adherent to the Crofer22APU and despite its reduced thickness (~3.5 µm), its high densification guaranteed the protection of the steel during the long term test. This is confirmed by the good performance demonstrated by 10CuMCO in the oxidation resistance test discussed above.

Figure 6 HERE

Fig. 6. *Cross section SEM images of the coated samples after different aging periods: as-sintered (a, b and c), after 1000h (d, e and f) and after 3000h (g, h and i).*

A more detailed analysis of the 10CuMCO sample after 3000 hours oxidation is shown in **Fig. 7**. EDS mapping shows a homogeneous distribution of the elements throughout the coating. Chromium does not seem to be present inside the coating, even close to the chromia interface the signal is within an experimental error with no visible Cr peak in the EDS spectra. Elemental map of Cr element shows its enrichment at the steel/coating interface due to formation of the chromia scale. Chemical analysis of the layers beneath and above the crack shows very similar composition of the two layers. EDS point analyses reported in **Fig. 7** confirms the good stability of Cu in the spinel; the Cu/(Mn+Co+Cu) ratio results 0.1 for point 1 and 0.08 for point 2 (almost identical to the theoretical value previously calculated). Moreover, the Mn/Co ratio in the aged coating is ~1.2 instead of the initial 1.0: as discussed earlier, this Mn enrichment in the spinel could be due to its diffusion from the steel (which contains ~0.5 wt.% of Mn in its composition).

Figure 7 HERE

Fig. 7. EDS analysis (elemental maps) of 10CuMCO sample after 3000h oxidation at 800 °C

3.4. Area Specific Resistance evaluation

In addition to corrosion exposure and post-mortem analysis, the electrical resistance of coated interconnect steels was measured over a long period of time (total of ~3600 hours, with few unintentional breaks). Development of the ASR as a function of time is presented in **Fig. 8A**. All the samples showed an initial high ASR value with a fast drop in the first 250h of test, this was due to the consolidation and sintering of LSM contact paste and plate on each sample. The fired LSM plate undergoes sintering as presented in previous studies [19,34]. The not coated steel has the largest initial ASR value, which has also been observed previously. It is believed to originate in a worse electrical contact/current restriction issues between the steel/contacting plate than in the case of steels with well conducting ceramic protective coatings. The ASR increases (taking into account a linear extrapolation) at a higher rate than for the coated samples (~3.6 mΩ cm^2 per 1000 hours). Among the coated samples, the results are very similar, the small difference being possibly due to minor experimental differences (contact area). The coated alloys are characterized by a roughly 3x slower ASR increase rate, which is important for the long term performance of the stacks. By a simple linear extrapolation (representing the worst case scenario), the ASR after 40000 can be calculated to be ~160 mΩ cm^2 for the uncoated sample and ~66 mΩ cm^2 for the coated samples, remaining below the often cited limit of 100 mΩ cm^2 [48]. Clearly the coating can

make a large difference in the resistance introduced by the interconnect to the total resistance of the stack.

From the ASR data collected during the cooling phase, presented in **Fig. 8B**, the activation energy for the electrical conduction process can be calculated according to the Arrhenius equation (according to modified Equation 1). All samples show quite similar activation energy values with a characteristic change of slopes in the intermediate temperature. In the high temperature region (500 °C-800 °) the activation energy is in the range 0.8-0.9 eV whereas in the low temperature region the activation energy is ~0.4-0.6 eV. These values correspond well to the values reported in the literature. Talic et al. [19] reported values in the range ~0.8 eV for Fe/Cu doped spinel on Crofer 22 APU. Kruk et al. [49] have shown activation energies ~0.7 eV also for quite similar system. Grolig et al. [50] have shown that the obtained activation energy might depend on the experimental conditions, but the values were still in the range of 05 – 0.85 eV. The electrical conductivity of the oxidized coated alloys shows visibly activation energy than the activation energy of bulk spinel materials (as reported in section 3.1) due to the resistance of the chromia layer. The similar values of the ASR and activation energy obtained upon cooling might be due to the negligible effect of the coating on the total cross-scale conductivity, dominated by a much worse conducting chromia layer, which forms in all cases. As the measured weight gain was quite similar for all coated samples, the chromia scale thickness and its electrical resistance can be expected to be similar, thus resulting in the similar conductivity vs. temperature behaviour.

Figure 8 HERE

Fig. 8. *ASR development as a function of time (A) and Arrhenius plot for calculation of activation energy (B).*

4. Conclusions

This work showed that it is possible to produce in-situ Cu-doped MnCo spinels, by a single-step electrophoretic co-deposition followed by reactive sintering. The proposed method allowed to deposit ceramic coatings with controlled chemical composition and desired ratio of phases. Cu doping of MnCo spinels reduced the extent of the tetragonal-cubic phase transition thus limiting possible thermal stresses due to mismatch of coefficients of thermal expansion. Addition of Cu lowers the temperature of the reduction step by ~100 °C. Coatings with closed porosity could be processed at 900 °C instead of 1000 °C, thus limiting the initial oxidation of the interconnects. The long term evaluation of the Cu-doped MnCo spinels coated Crofer22APU samples, tested up to

3000 hrs at 800°C, demonstrated an increased densification together with the stability of the copper inside the spinels. Corrosion rate of the interconnects with Cu-doped protective coatings was found to be ~10x lower than for the uncoated ones, showing virtually no diffusion of chromium, thus remaining protective. The findings of this study suggest that proposed approach can be further expanded to study incorporation of other transition metals into the spinel structure. By proper selection of in-situ dopant, the electrical conductivity and thermal expansion coefficients can be potentially tailored for different steel substrates.

Acknowledgements

F. S., A. G. S. and A. R. B. would like to acknowledge the funding from KMM-VIN http://www.kmm-vin.eu/home/ fellowships (7th call) granted to Dr. Antonio Gianfranco Sabato.

S.M. would like to acknowledge the funding from the National Science Centre Poland (NCN) project Harmonia: "Quest for novel materials for solid oxide cell interconnect coatings" 2018-2021 and Statutory Funds of the WETI PG. Justyna Ignaczak is acknowledged for help with electrical measurements of pellets.

Figure Captions

Figure 1 SEM images of a) MCO and b) CuO powders used for the co-deposition.

Figure 2 Results of electrical conductivity (σ) collected on the pellets of MCO and 10CuMCO: σ and T vs. time (a and b), σ vs. T (c) and Arrhenius plots (d).

Figure 3 Results of oxidation resistance test at 800°C in air: weight gain vs. time (a), weight gain squared vs. time (b) and instantaneous corrosion rate vs. time (c) for bare Crofer22APU (reference) and MCO, 5CuMCO, 10CuMCO coated samples.

Figure 4 XRD indexed patterns for MCO (a), 5CuMCO (b) and 10CuMCO (c) collected after aging for 0h, 1000h, 3000h together with a magnification (2θ 28°-40°) of the spectra of MCO and 10CuMCO (d).

Figure 5 SEM images (top-view) of coated samples after different aging periods (0h, 1000h, 3000h): MCO (A, B, C), 5CuMCO (D, E, F) and 10CuMCO (G, H, I).

Figure 6 Cross section SEM images of the coated samples after different aging periods: as-sintered (a, b and c), after 1000h (d, e and f) and after 3000h (g, h and i).

Figure 7 EDS analysis (elemental maps) of 10CuMCO sample after 3000h oxidation at 800 °C

Figure 8 ASR development as a function of time (A) and Arrhenius plot for calculation of activation energy (B).

Tables

Table 1 Corrosion rates (k_p) calculated from the slope of the weight gain curves shown in **Fig. 3B**.

Table 2 Results of EDS semi-quantitative analyses collected on the surfaces of the coated samples reported in **Fig. 5**.

References

[1] S.C. Singhal, Solid oxide fuel cells for stationary, mobile, and military applications, Solid State Ionics. 152–153 (2002) 405–410. doi:10.1016/S0167-2738(02)00349-1.

[2] S.C. Singhal, K. Kendall, High-temperature solid oxide fuel cells: fundamentals, design, and applicatons, 2003.

[3] J.W. Fergus, Metallic interconnects for solid oxide fuel cells, Mater. Sci. Eng. A. 397 (2005) 271–283. doi:10.1016/j.msea.2005.02.047.

[4] M.A. Laguna-Bercero, Recent advances in high temperature electrolysis using solid oxide fuel cells: A review, J. Power Sources. 203 (2012) 4–16. doi:10.1016/j.jpowsour.2011.12.019.

[5] V.N. Nguyen, Q. Fang, U. Packbier, L. Blum, Long-term tests of a Ju ¨ lich planar short stack with reversible solid oxide cells in both fuel cell and electrolysis modes, Int. J. Hydrogen Energy. 38 (2013) 4281–4290. doi:10.1016/j.ijhydene.2013.01.192.

[6] N. Mahato, A. Banerjee, A. Gupta, S. Omar, K. Balani, Progress in material selection for solid oxide fuel cell technology: A review, Prog. Mater. Sci. 72 (2015) 141–337. doi:10.1016/j.pmatsci.2015.01.001.

[7] J.C.W. Mah, A. Muchtar, M.R. Somalu, M.J. Ghazali, Metallic interconnects for solid oxide fuel cell: A review on protective coating and deposition techniques, Int. J. Hydrogen Energy. 42 (2017) 9219–9229. doi:10.1016/j.ijhydene.2016.03.195.

[8] N. Shaigan, W. Qu, D.G. Ivey, W. Chen, A review of recent progress in coatings, surface modifications and alloy developments for solid oxide fuel cell ferritic stainless steel interconnects, J. Power Sources. 195 (2010) 1529–1542. doi:10.1016/j.jpowsour.2009.09.069.

[9] G.A. Ludwig, M.A. Korb, D.A.S. Lima, M.A. Macías, G.H. Gauthier, C.F. Malfatti, Protective coatings for AISI 430 stainless steel at high temperatures using perovskite oxides La0.6Sr0.4CoO3 on spinel type oxide NiFe2O4, Ceram. Int. 41 (2015) 14561–14573. doi:10.1016/j.ceramint.2015.07.173.

[10] I. Belogolovsky, P.Y. Hou, C.P. Jacobson, S.J. Visco, Chromia scale adhesion on 430 stainless steel: Effect of different surface treatments, J. Power Sources. 182 (2008) 259–264. doi:10.1016/j.jpowsour.2008.03.080.

[11] W.N. Liu, X. Sun, E. Stephens, M. Khaleel, Effect of substrate thickness on oxide scale spallation for solid oxide fuel cells, Corros. Sci. 53 (2011) 2406–2412. doi:10.1016/j.corsci.2011.03.025.

[12] S. Molin, A.G. Sabato, M. Bindi, P. Leone, G. Cempura, M. Salvo, S. Cabanas Polo, A.R. Boccaccini, F. Smeacetto, Microstructural and electrical characterization of Mn-Co spinel protective coatings for solid oxide cell interconnects, J. Eur. Ceram. Soc. 37 (2017) 4781–4791. doi:10.1016/j.jeurceramsoc.2017.07.011.

[13] K. Wang, Y. Liu, J.W. Fergus, Interactions Between SOFC Interconnect Coating Materials and Chromia, J. Am. Ceram. Soc. 94 (2011) 4490–4495. doi:10.1111/j.1551-2916.2011.04749.x.

[14] S.P. Jiang, X. Chen, Chromium deposition and poisoning of cathodes of solid oxide fuel cells – A review, Int. J. Hydrogen Energy. 39 (2014) 505–531. doi:10.1016/j.ijhydene.2013.10.042.

[15] Z. Yang, M. Guo, N. Wang, C. Ma, J. Wang, M. Han, A short review of cathode poisoning and corrosion in solid oxide fuel cell, Int. J. Hydrogen Energy. 42 (2017) 24948–24959. doi:10.1016/j.ijhydene.2017.08.057.

[16] M. Krumpelt, T.A. Cruse, B.J. Ingram, J.L. Routbort, S. Wang, P.A. Salvador, G. Chen, The Effect of Chromium Oxyhydroxide on Solid Oxide Fuel Cells, J. Electrochem. Soc. . 157 (2010) B228–B233. doi:10.1149/1.3266930.

[17] A. Petric, H. Ling, Electrical Conductivity and Thermal Expansion of Spinels at Elevated Temperatures, J. Am. Ceram. Soc. 90 (2007) 1515–1520. doi:10.1111/j.1551-2916.2007.01522.x.

[18] Z. Yang, G.G. Xia, X.H. Li, J.W. Stevenson, (Mn,Co)3O4 spinel coatings on ferritic stainless steels for SOFC interconnect applications, Int. J. Hydrogen Energy. 32 (2007) 3648–3654. doi:10.1016/j.ijhydene.2006.08.048.

[19] B. Talic, S. Molin, K. Wiik, P.V.P.V. Hendriksen, H.L. Lein, Comparison of iron and copper doped manganese cobalt spinel oxides as protective coatings for solid oxide fuel cell interconnects, J. Power Sources. 372 (2017) 145–156. doi:10.1016/j.jpowsour.2017.10.060.

[20] B. Talic, H. Falk-Windisch, V. Venkatachalam, P.V. Hendriksen, K. Wiik, H.L. Lein, Effect of coating density on oxidation resistance and Cr vaporization from solid oxide fuel cell interconnects, J. Power Sources. 354 (2017) 57–67. doi:10.1016/j.jpowsour.2017.04.023.

[21] S. Molin, Evaluation of electrodeposited Mn-Co protective coatings on Crofer 22 APU steel, Internationa Journal of Applied Ceramic Technology (2017) 349–360. doi:10.1111/ijac.12816.

[22] S. Molin, A.G. Sabato, H. Javed, G. Cempura, A.R. Boccaccini, F. Smeacetto, Co-deposition of CuO and Mn 1 . 5 Co 1 . 5 O 4 powders on Crofer22APU by electrophoretic

method : Structural , compositional modifications and corrosion properties, Materials Letters 218 (2018) 329–333.

[23] M. Bobruk, S. Molin, M. Chen, T. Brylewski, P.V. Hendriksen, Sintering of MnCo2O4coatings prepared by electrophoretic deposition, Mater. Lett. 213 (2018) 394–398.

[24] H. Zhang, Z. Zhan, X. Liu, Electrophoretic deposition of (Mn,Co)3O4 spinel coating for solid oxide fuel cell interconnects, J. Power Sources. 196 (2011) 8041–8047. doi:10.1016/j.jpowsour.2011.05.053.

[25] F. Smeacetto, A. De Miranda, S. Cabanas Polo, S. Molin, D. Boccaccini, M. Salvo, A.R. Boccaccini, Electrophoretic deposition of Mn1.5Co1.5O4on metallic interconnect and interaction with glass-ceramic sealant for solid oxide fuel cells application, J. Power Sources. 280 (2015) 379–386.

[26] H. Abdoli, P. Alizadeh, Electrophoretic deposition of (Mn,Co) 3O 4 spinel nano powder on SOFC metallic interconnects, Mater. Lett. 80 (2012) 53–55. doi:10.1016/j.matlet.2012.04.072.

[27] L. Besra, M. Liu, A review on fundamentals and applications of electrophoretic deposition (EPD), Prog. Mater. Sci. 52 (2007) 1–61. doi:10.1016/j.pmatsci.2006.07.001.

[28] A.R. Boccaccini, I. Zhitomirsky, Application of electrophoretic and electrolytic deposition techniques in ceramics processing - Part 2, InterCeram Int. Ceram. Rev. 54 (2005) 242–246. doi:10.1016/S1359-0286(02)00080-3.

[29] I. Corni, M.P. Ryan, A.R. Boccaccini, Electrophoretic deposition: From traditional ceramics to nanotechnology, J. Eur. Ceram. Soc. 28 (2008) 1353–1367. doi:10.1016/j.jeurceramsoc.2007.12.011.

[30] M. Mirzaei, A. Simchi, M.A. Faghihi-Sani, A. Yazdanyar, Electrophoretic deposition and sintering of a nanostructured manganese-cobalt spinel coating for solid oxide fuel cell interconnects, Ceram. Int. 42 (2016) 6648–6656. doi:10.1016/j.ceramint.2016.01.012.

[31] Y. Xu, Z. Wen, S. Wang, T. Wen, Cu doped Mn–Co spinel protective coating on ferritic stainless steels for SOFC interconnect applications, Solid State Ionics. 192 (2011) 561–564. doi:10.1016/j.ssi.2010.05.052.

[32] J. Xiao, W. Zhang, C. Xiong, B. Chi, J. Pu, L. Jian, Oxidation behavior of Cu-doped MnCo2O4 spinel coating on ferritic stainless steels for solid oxide fuel cell interconnects, Int. J. Hydrogen Energy. 41 (2016) 9611–9618. doi:10.1016/j.ijhydene.2016.03.051.

[33] D. Szymczewska, S. Molin, P. Hendriksen, P. Jasiński, Microstructure and Electrical Properties of Fe,Cu Substituted (Co,Mn)3O4 Thin Films, Cryst. 2017, Vol. 7, Page 185. 7

(2017) 185. doi:10.3390/CRYST7070185.

[34] S. Molin, P. Jasinski, L. Mikkelsen, W. Zhang, M. Chen, P. V. Hendriksen, Low temperature processed MnCo2O4and MnCo1.8Fe0.2O4as effective protective coatings for solid oxide fuel cell interconnects at 750 ï¿½C, J. Power Sources. 336 (2016) 408–418. doi:10.1016/j.jpowsour.2016.11.011.

[35] B.K. Park, J.W. Lee, S.B. Lee, T.H. Lim, S.J. Park, C.O. Park, R.H. Song, Cu- and Ni-doped Mn1.5Co1.5O4spinel coatings on metallic interconnects for solid oxide fuel cells, Int. J. Hydrogen Energy. 38 (2013) 12043–12050. doi:10.1016/j.ijhydene.2013.07.025.

[36] A. Masi, M. Bellusci, M. Carlini, S.J. McPhail, F. Padella, P. Reale, Mechanochemical Processing of Mn and Co Oxides: An Alternative Way to Synthesize Mixed Spinels for Protective Coating, J. Am. Ceram. Soc. 99 (2015) n/a-n/a. doi:10.1111/jace.13863.

[37] A. Masi, M. Bellusci, S.J. McPhail, F. Padella, P. Reale, J.-E. Hong, R. Steinberger-Wilckens, M. Carlini, Cu-Mn-Co oxides as protective materials in SOFC technology: The effect of chemical composition on mechanochemical synthesis, sintering behaviour, thermal expansion and electrical conductivity, J. Eur. Ceram. Soc. 37 (2017) 661–669. doi:10.1016/j.jeurceramsoc.2016.09.025.

[38] J.C.W. Mah, A. Muchtar, M.R. Somalu, M.J. Ghazali, Formation of sol – gel derived (Cu , Mn , Co) 3 O 4 spinel and its electrical properties, Ceram. Int. 43 (2017) 7641–7646. doi:10.1016/j.ceramint.2017.03.060.

[39] T. Brylewski, A. Kruk, M. Bobruk, A. Adamczyk, J. Partyka, P. Rutkowski, Structure and electrical properties of Cu-doped Mn-Co-O spinel prepared via soft chemistry and its application in intermediate-temperature solid oxide fuel cell interconnects, J. Power Sources. 333 (2016) 145–155. doi:10.1016/j.jpowsour.2016.09.136.

[40] J. Xiao, W. Zhang, C. Xiong, B. Chi, J. Pu, L. Jian, Oxidation of MnCu0.5Co1.5O4 spinel coated SUS430 alloy interconnect in anode and cathode atmospheres for intermediate temperature solid oxide fuel cell, Int. J. Hydrogen Energy. 40 (2014) 1868–1876. doi:10.1016/j.ijhydene.2014.11.124.

[41] N. Hosseini, F. Karimzadeh, M.H. Abbasi, G.M. Choi, Microstructural characterization and electrical conductivity of Cu xMn3-xO4 (0.9≤x≤1.3) spinels produced by optimized glycine-nitrate combustion and mechanical milling processes, Ceram. Int. 40 (2014) 12219–12226. doi:10.1016/j.ceramint.2014.04.065.

[42] N.S. Waluyo, S.S. Park, R.H. Song, S.B. Lee, T.H. Lim, J.E. Hong, K.H. Ryu, W. Bin Im, J.W. Lee, Protective coating based on manganese–copper oxide for solid oxide fuel cell

interconnects: Plasma spray coating and performance evaluation, Ceram. Int. 44 (2018) 11576–11581. doi:10.1016/j.ceramint.2018.03.220.

[43] A. Masi, M. Bellusci, S.J. McPhail, F. Padella, P. Reale, J.-E. Hong, R. Steinberger-Wilckens, M. Carlini, The effect of chemical composition on high temperature behaviour of Fe and Cu doped Mn-Co spinels, Ceram. Int. 43 (2017) 2829–2835. doi:10.1016/j.ceramint.2016.11.135.

[44] C. Goebel, A.G. Fefekos, J.E. Svensson, J. Froitzheim, Does the conductivity of interconnect coatings matter for solid oxide fuel cell applications?, J. Power Sources. 383 (2018) 110–114. doi:10.1016/j.jpowsour.2018.02.060.

[45] T. Brylewski, W. Kucza, A. Adamczyk, A. Kruk, M. Stygar, M. Bobruk, J. Dąbrowa, Microstructure and electrical properties of Mn1+xCo2−xO4 (0≤x≤1.5) spinels synthesized using EDTA-gel processes, Ceram. Int. 40 (2014) 13873–13882. doi:10.1016/j.ceramint.2014.05.106.

[46] B. Talic, P.V. Hendriksen, K. Wiik, H.L. Lein, Thermal expansion and electrical conductivity of Fe and Cu doped MnCo2O4spinel, Solid State Ionics. 326 (2018) 90–99. doi:10.1016/j.ssi.2018.09.018.

[47] H. Bordeneuve, C. Tenailleau, S. Guillemet-Fritsch, R. Smith, E. Suard, A. Rousset, Structural variations and cation distributions in Mn3-xCoxO4(0 ≤ x ≤ 3) dense ceramics using neutron diffraction data, Solid State Sci. 12 (2010) 379–386. doi:10.1016/j.solidstatesciences.2009.11.018.

[48] B.C.H. Steele, Survey of materials selection for ceramic fuel cells, Solid State Ionics. 88 (1996) 1223–1234.

[49] A. Kruk, M. Stygar, T. Brylewski, Mn-Co spinel protective-conductive coating on AL453 ferritic stainless steel for IT-SOFC interconnect applications, J. Solid State Electrochem. (2013). doi:10.1007/s10008-012-1952-8.

[50] J.G. Grolig, J. Froitzheim, J.-E. Svensson, Coated stainless steel 441 as interconnect material for solid oxide fuel cells: Evolution of electrical properties, J. Power Sources. 284 (2015) 321–327. doi:10.1016/j.jpowsour.2015.03.029.

Figure 1

Click here to download high resolution image

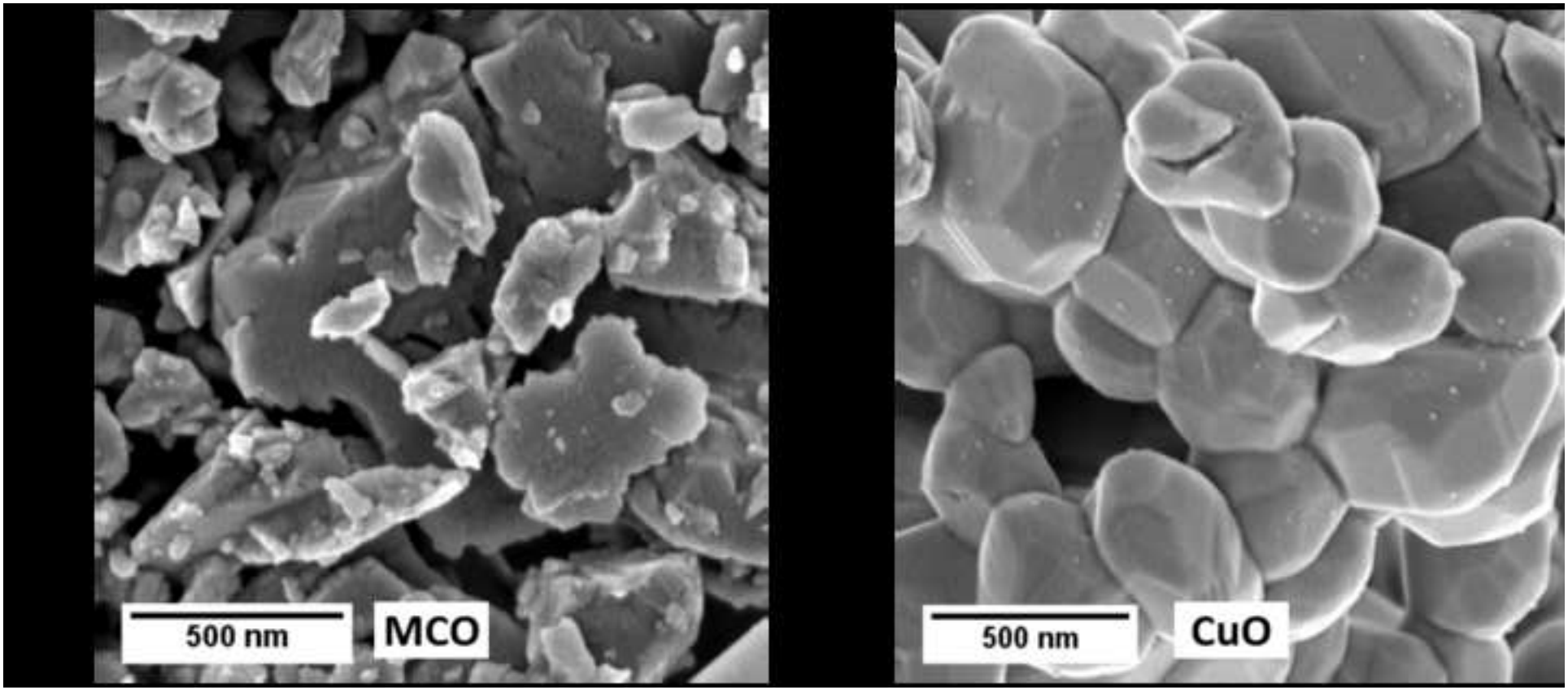

Figure 2

Click here to download high resolution image

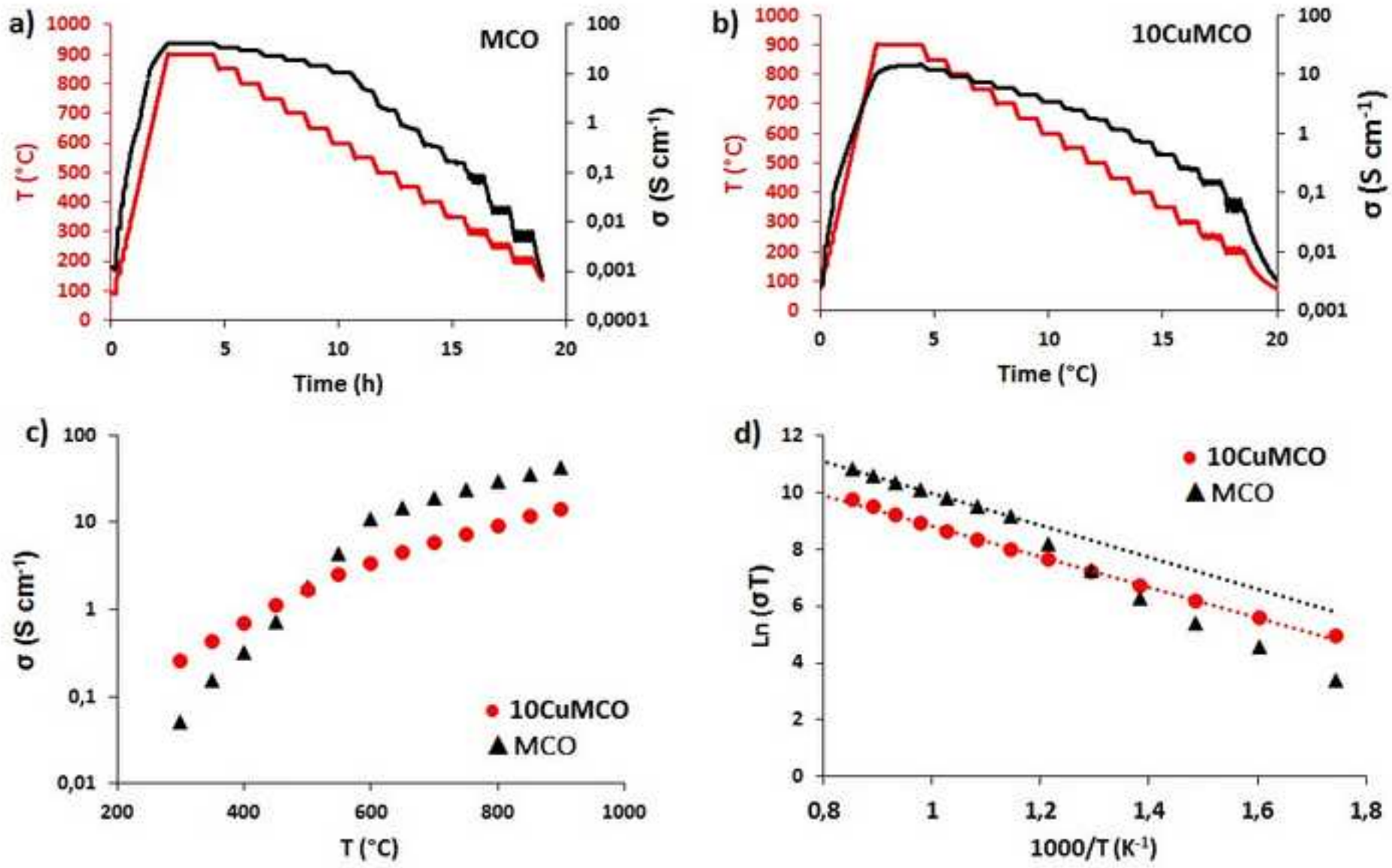

Figure 3 revised

Click here to download high resolution image

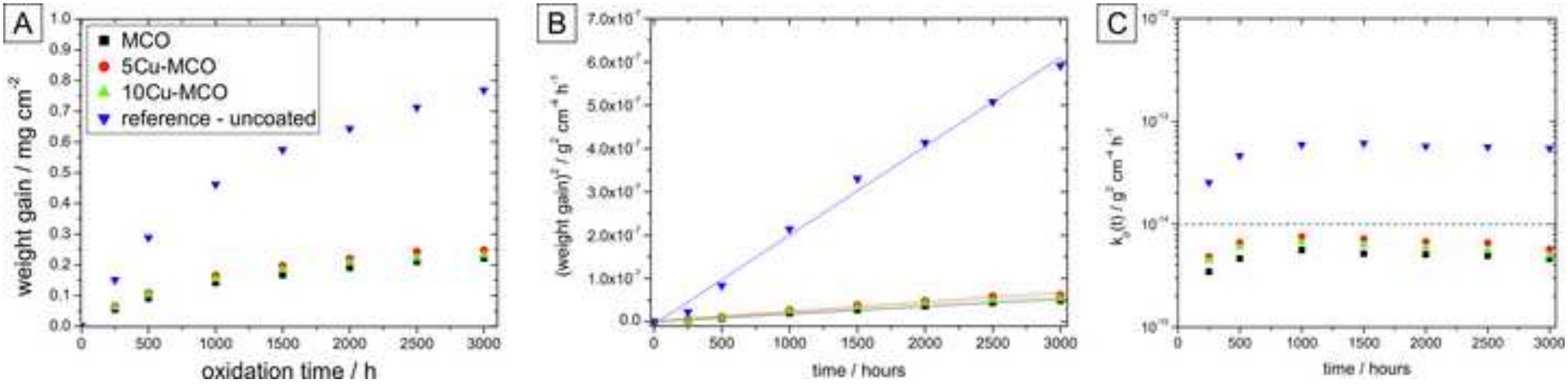

Figure 4

Click here to download high resolution image

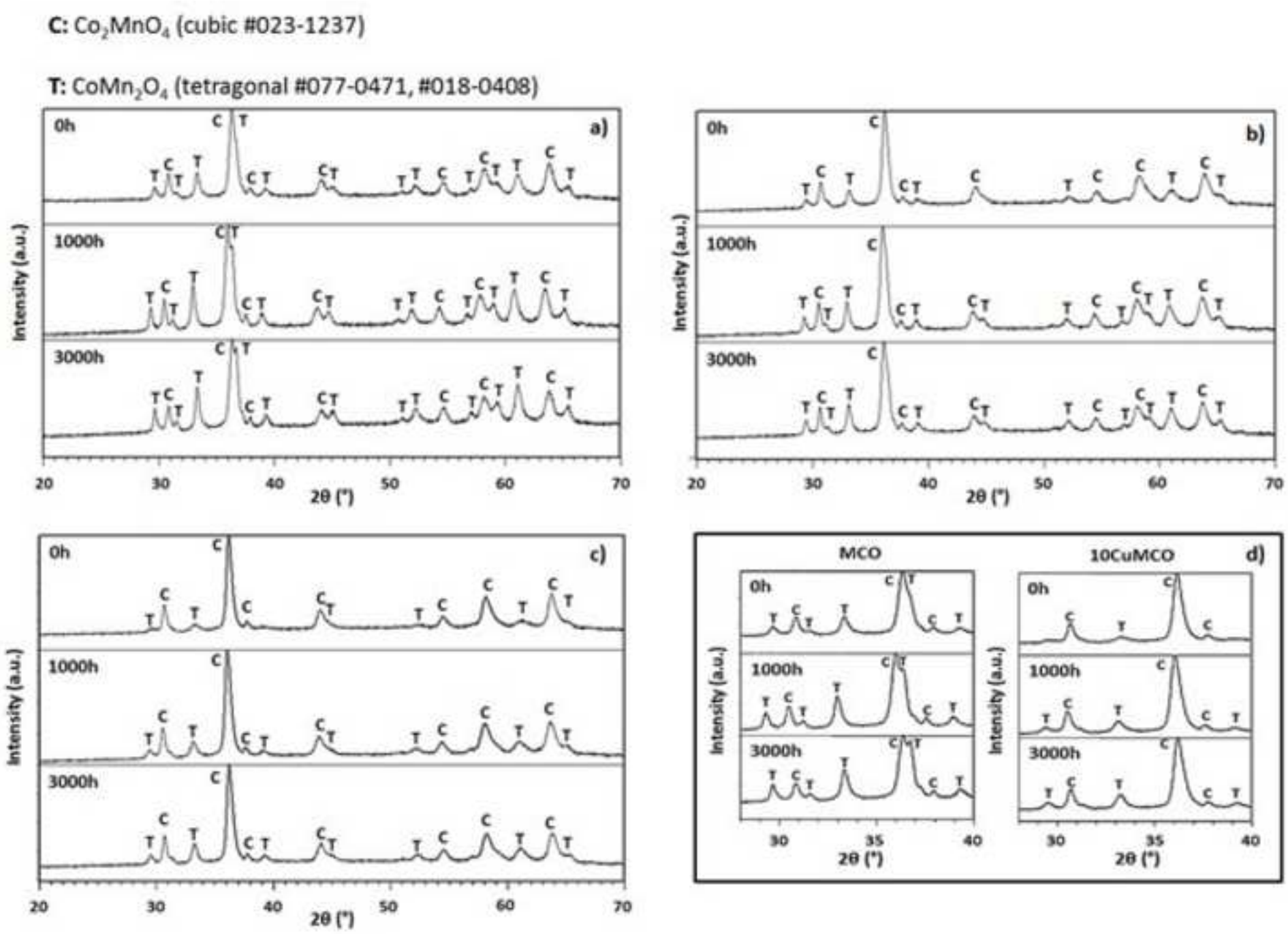

Figure 5

Click here to download high resolution image

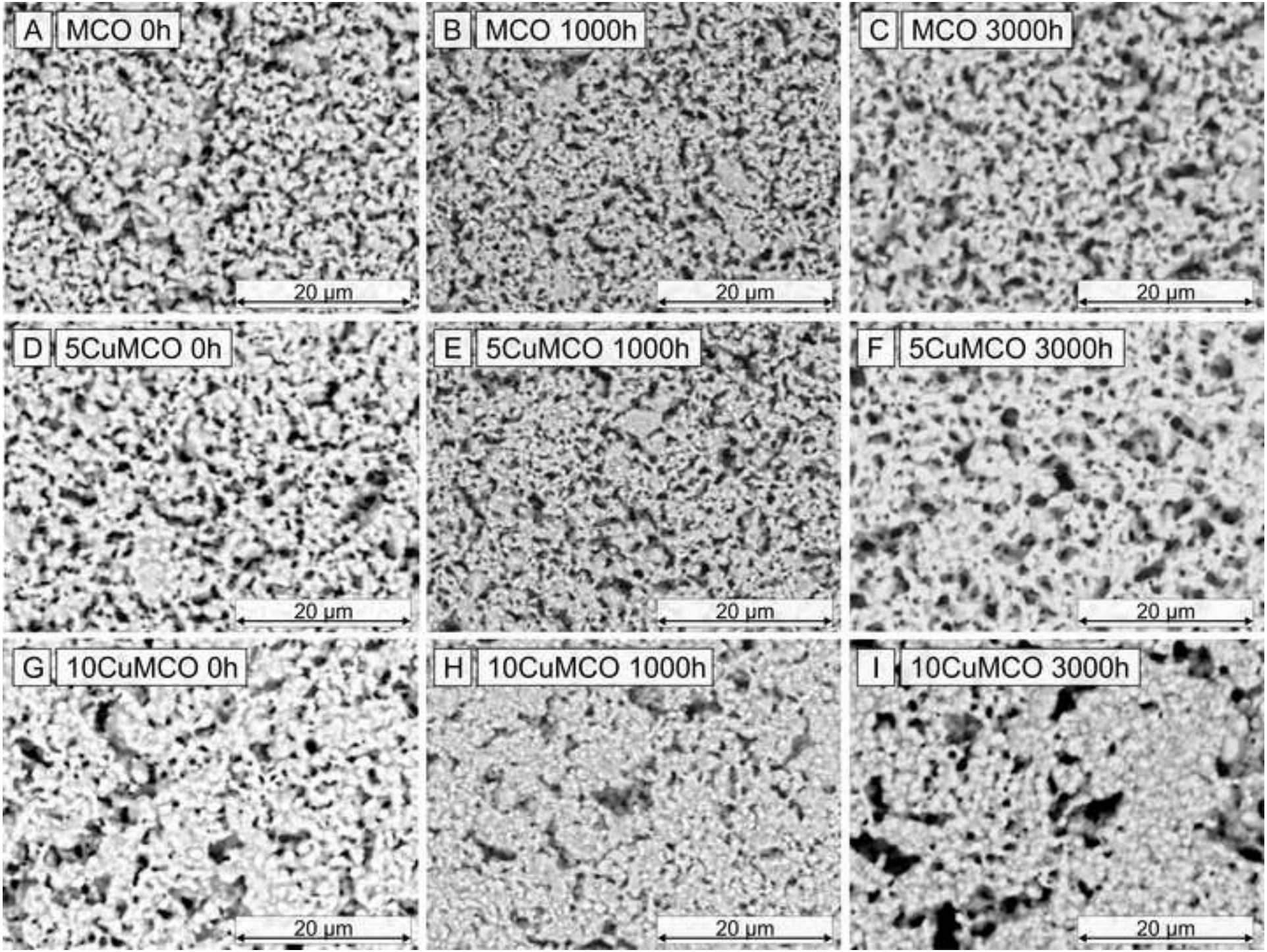

Figure 6

Click here to download high resolution image

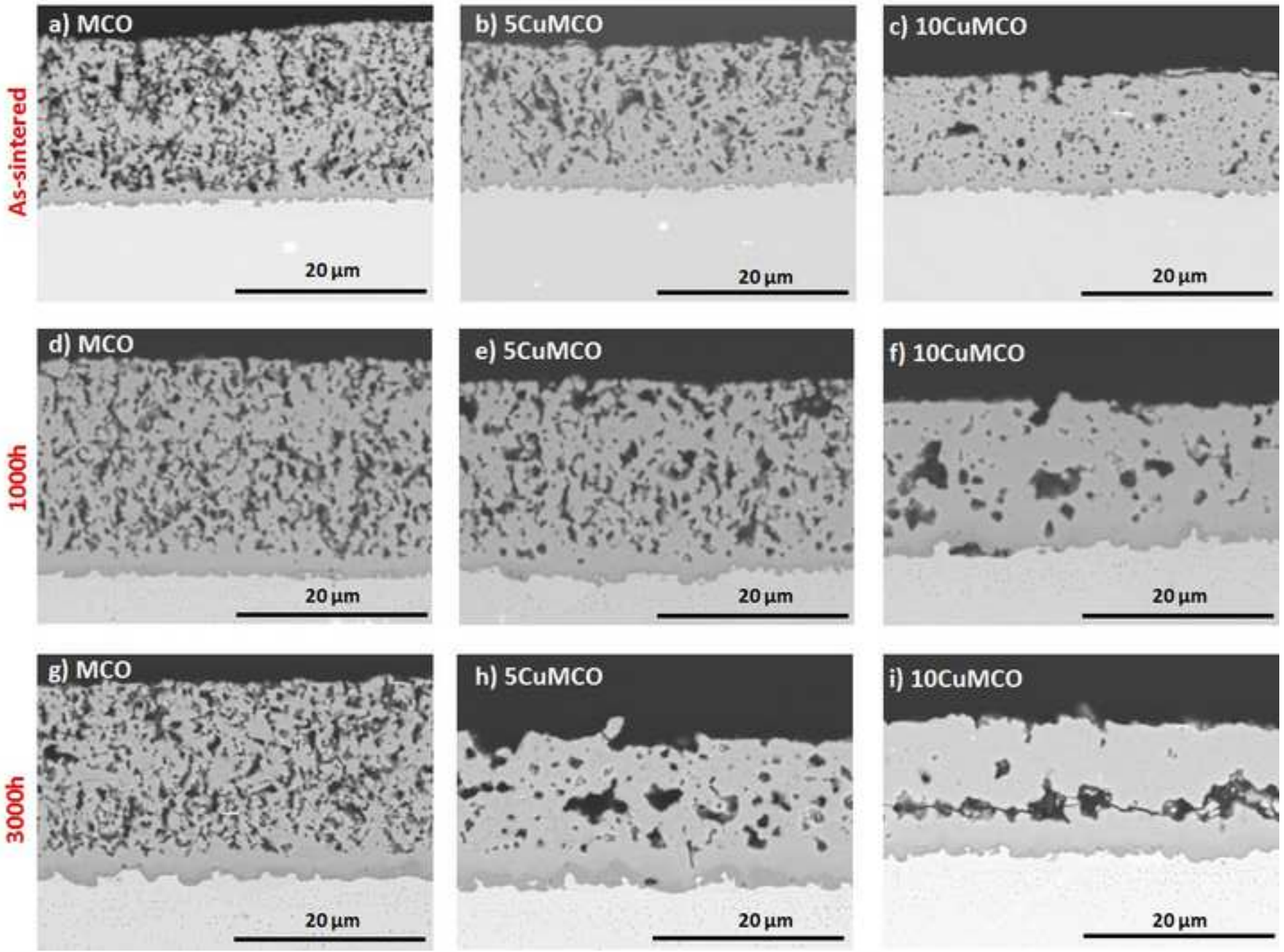

Figure 7

Click here to download high resolution image

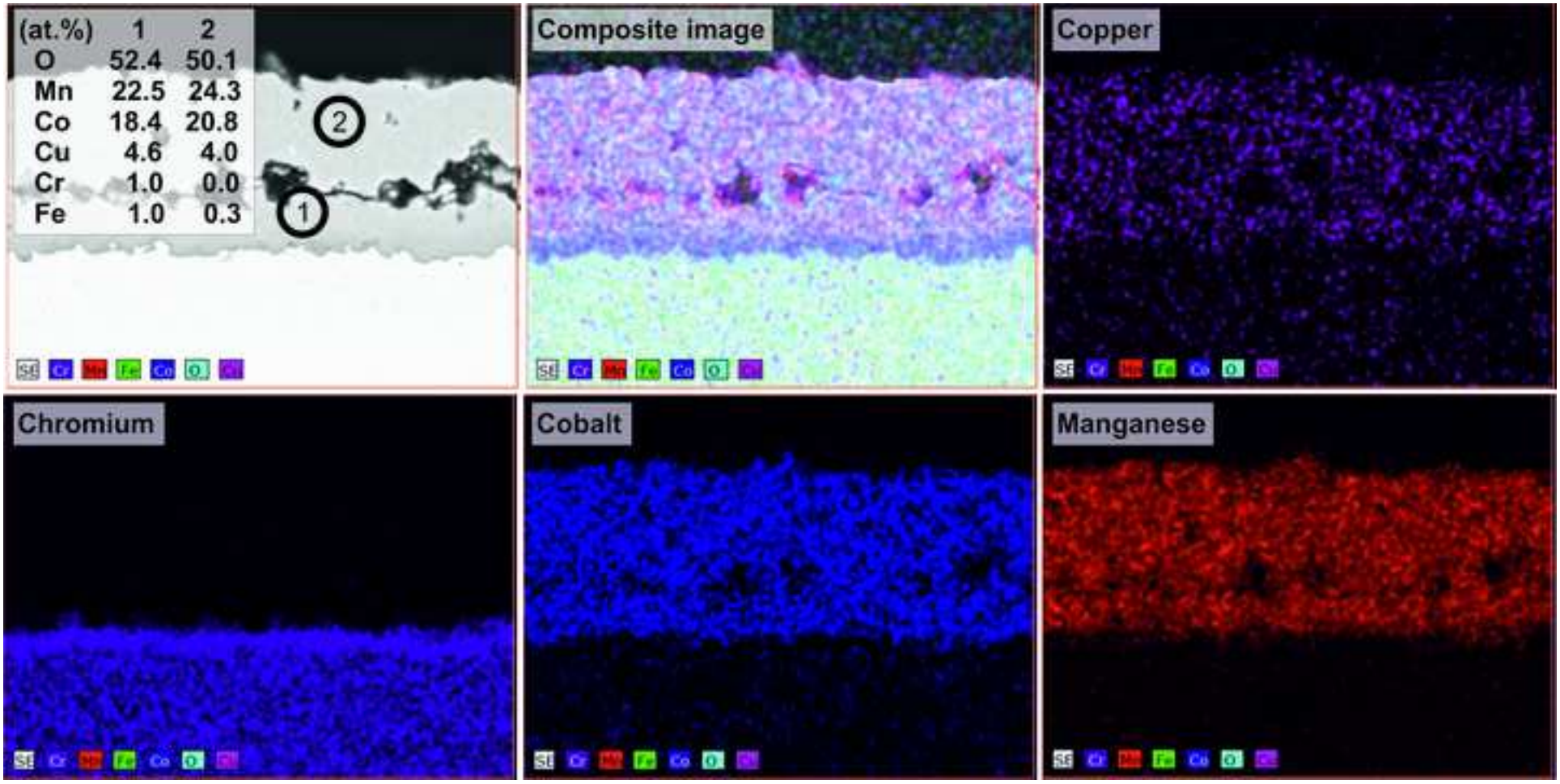

Figure 8

Click here to download high resolution image

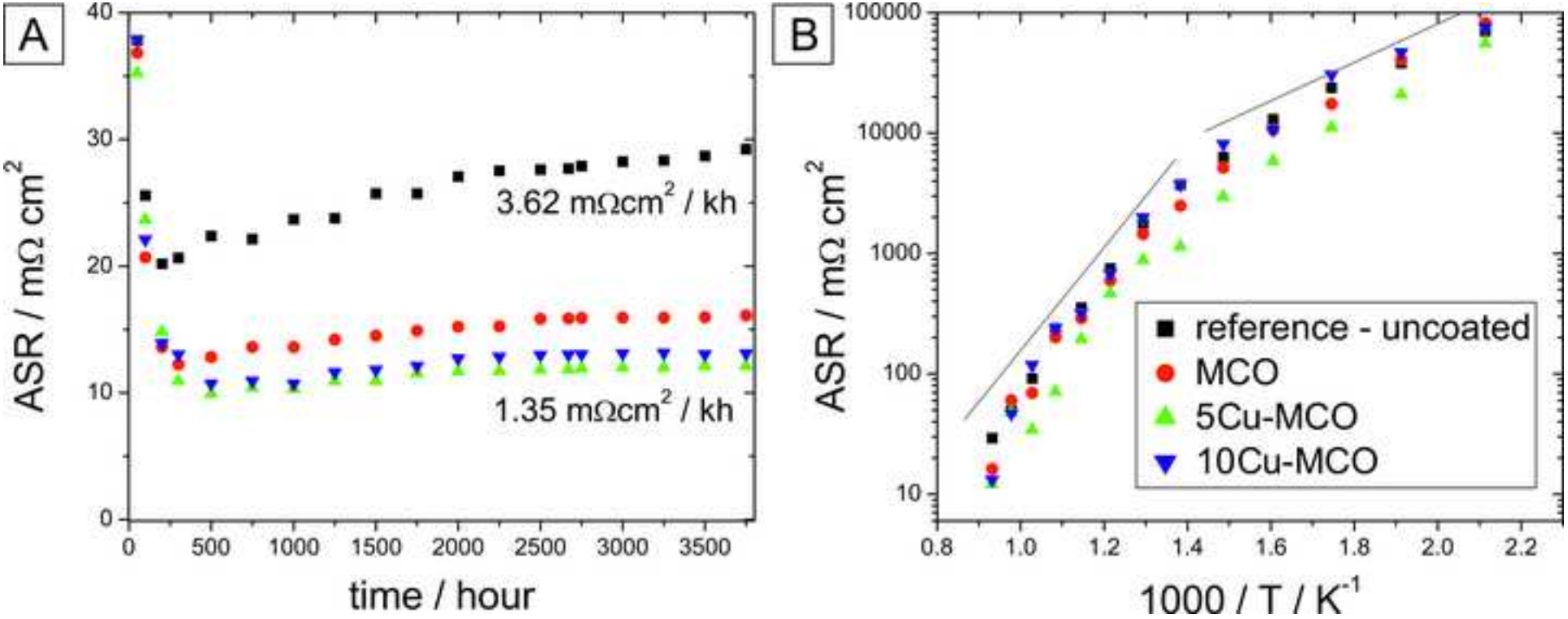

Table 1

Sample:	Corrosion rate value [$x10^{-14}$ g^2 cm^{-4} s^{-1}]
MCO	0.53
5CuMCO	0.71
10CuMCO	0.62
Reference	6.11

Table 2

At%	MCO			5CuMCO			10CuMCO		
	0h	1000h	3000h	0h	1000h	3000h	0h	1000h	3000h
O	55.7	51	54.6	54.1	51.4	53.9	55	53	52.1
Co	23	23.2	21.1	22.1	21.7	19.7	20.7	20.4	19.7
Mn	21.3	25.1	23.7	20.4	24.3	23.7	20.1	22	23.4
Cu	-	-	-	3	2.1	1.9	3.8	4.3	4.1
Cr	-	0.3	-	0.1	0.3	0.4	0.1	0.3	0.2
Fe	-	0.4	0.6	0.3	0.2	0.4	0.3	0.4	0.5
Mn/Co	0.92	1.08	1.12	0.92	1.12	1.2	0.97	1.08	1.19
Cu/(Mn+Co+Cu)	-	-	-	0.066	0.044	0.042	0.085	0.092	0.087